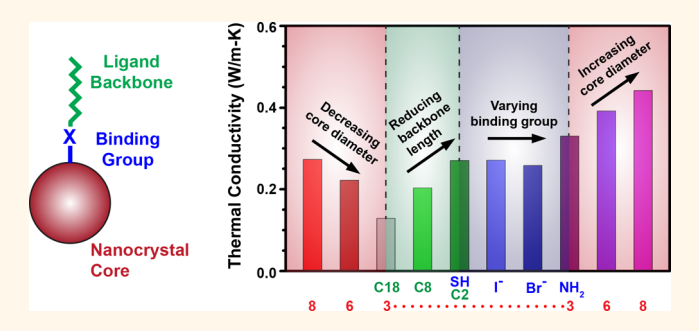
Modifying Thermal Transport in Colloidal Nanocrystal Solids with Surface Chemistry

Minglu Liu, Yuanyu Ma, and Robert Y. Wang*

School for Engineering of Matter, Transport & Energy, Arizona State University, Tempe, Arizona 85287, United States

ABSTRACT We present a systematic study on the effect of surface chemistry on thermal transport in colloidal nanocrystal (NC) solids. Using PbS NCs as a model system, we vary ligand binding group (thiol, amine, and atomic halides), ligand length (ethanedithiol, butanedithiol, hexanedithiol, and octanedithiol), and NC diameter (3.3—8.2 nm). Our experiments reveal several findings: (i) The ligand choice can vary the NC solid thermal conductivity by up to a factor of 2.5. (ii) The ligand binding strength to the NC core does not significantly impact thermal conductivity.



(iii) Reducing the ligand length can decrease the interparticle distance, which increases thermal conductivity. (iv) Increasing the NC diameter increases thermal conductivity. (v) The effect of surface chemistry can exceed the effect of NC diameter and becomes more pronounced as NC diameter decreases. By combining these trends, we demonstrate that the thermal conductivity of NC solids can be varied by an overall factor of 4, from \sim 0.1-0.4 W/m-K. We complement these findings with effective medium approximation modeling and identify thermal transport in the ligand matrix as the rate-limiter for thermal transport. By combining these modeling results with our experimental observations, we conclude that future efforts to increase thermal conductivity in NC solids should focus on the ligand—ligand interface between neighboring NCs.

KEYWORDS: colloidal nanocrystal · ligand · nanocrystal solid · thermal conductivity · thermal transport

olloidal nanocrystals (NCs) are an important class of nanoparticle that can shape, and composition. This morphological control enables excellent control over NC properties and facilitates their use as building blocks for nanocomposites with novel and tunable properties that are unachievable in bulk materials. 1-3 One commonly studied NC-based material is the colloidal NC solid, which consists of a densely packed array of colloidal NCs. These colloidal NC solids have been employed across a wide range of applications including light emitting diodes (LEDs),^{4,5} photovoltaics,^{6,7} electronics,^{8,9} thermal storage,^{3,10} and thermoelectrics.^{11,12} In each of these applications, thermal transport properties play an important role. For example, a high thermal conductivity is desirable for LEDs, photovoltaics, and electronics because this minimizes temperature rise during operation, which improves both device performance and lifetime. A high thermal conductivity is also beneficial for thermal storage because it facilitates fast thermal charging/ discharging. In contrast, a low thermal conductivity is ideal for thermoelectric applications because this improves efficiency in thermoelectric coolers and generators. Despite the importance of thermal conductivity in each of these applications, experimental data on thermal transport in NC solids is very limited.¹³

Colloidal NCs consist of an inorganic crystalline core with ligands bound to its surface. The native ligands on colloidal NCs are typically bulky organic molecules (e.g., oleic acid, trioctylphosphine oxide, alkanethiols, etc.). These native ligands help control the nucleation and growth of colloidal NCs during synthesis and are hence necessary from a synthetic perspective. However, these native ligands are generally undesirable from a functional materials perspective (e.g., electrically insulating). Previous studies have shown that the choice of ligands dramatically affects NC properties, 14-20 and it is now a common practice to replace

Received for review August 14, 2015 and accepted November 9, 2015.

Published online November 10, 2015 10.1021/acsnano.5b05085

© 2015 American Chemical Society

^{*} Address correspondence to rywang@asu.edu.

the native ligands with new ligands that impart desirable properties. For example, by replacing the native dodecanethiol ligands with metal chalcogenide complexes, the electrical conductivity of Au NC solids was increased by 10 orders of magnitude. ¹⁸ In another example, the optical absorption of PbS NCs was increased by a factor of 3 through the use of short conjugated ligands. ¹⁹ In addition to these intended effects on electrical and optical properties, it is important to understand how ligand choice affects thermal transport.

Thermal transport in NC solids was first experimentally studied by Ong et al.13 They found very low thermal conductivities and that NC diameter had the biggest impact on this property. They also conducted limited experiments on ligand-exchanged NC solids and found moderate thermal conductivity increases of \sim 50%. A couple of molecular dynamics studies have since confirmed the importance of NC diameter on thermal transport and also identified the NC coreligand interface as an important parameter. 21,22 While these studies are important landmarks in the study of thermal transport in NC solids, important questions regarding the effect of surface chemistry remain. How does the ligand's binding group and backbone length affect thermal transport in NC solids? Can ligand exchange increase NC solid thermal conductivity beyond the moderate 50% demonstrated by Ong et al.? How is the impact of surface chemistry on thermal transport affected by NC diameter?

To address these questions, we study thermal transport in PbS NC solids and systematically vary NC diameter and ligand structure. Our choice of PbS as a model system is motivated by the technological importance of PbS NC solids to optoelectronic applications, such as photodetectors^{6,23} and photovoltaics.^{7,16,24} In addition, PbS is among the most well understood colloidal NCs and there is a wide body of literature detailing its structure, 25,26 properties, 27,28 and behavior.^{29,30} The native ligands on the PbS NCs in this study are oleic acid (OA) and we exchange these with ligands of varying backbone length (ethanedithiol, butanedithiol, hexanedithiol and octanedithiol) and different binding groups (thiols, amines, and halides). Our experiments reveals several findings: (i) The choice of ligand can increase the thermal conductivity of NC solids by up to \sim 150%. (ii) The ligand binding strength to the NC core does not significantly impact thermal conductivity. (iii) Reducing the ligand length can decrease the interparticle distance, which increases thermal conductivity. (iv) Increasing the NC diameter increases thermal conductivity. (v) The effect of surface chemistry can exceed the effect of NC diameter and becomes more pronounced as NC diameter decreases. By combining these trends, we demonstrate that the thermal conductivity of NC solids can be varied by an overall factor of 4, from \sim 0.1-0.4 W/m-K. We complement these thermal

transport findings with effective medium approximation (EMA) modeling and identify thermal transport in the ligand matrix as the rate-limiting factor for heat transfer. By combining our experimental observations with these modeling results, we conclude that future efforts to increase thermal conductivity in NC solids should focus on the ligand—ligand interactions between neighboring NCs.

RESULTS AND DISCUSSION

We synthesized PbS NCs with OA ligands using the hot-injection method described by Hines et al.31 Figure 1b shows a representative transmission electron microscopy image of the PbS NCs made using this approach and X-ray diffraction confirms the crystalline structure of the PbS core (Figure 1d). Varying the reaction conditions enabled NC diameter control from 3.3 to 8.2 nm (Figure S5). After synthesis, the PbS NCs were spin-coated onto silicon substrates to yield a NC solid thin film (Figures 1a and 1c). The native OA ligands were then replaced with new ligands using a solid-state process. Seven different surface treatments were performed in this study: 1,2-ethanedithiol (EDT), 1,4-butanedithiol (BDT), 1,6-hexanedithiol (HDT), 1,8octanedithiol (ODT), ethylenediamine (EDA), tetrabutylammonium iodide (TBAI), and cetrimonium bromide (CTAB). The structures of these molecules are illustrated in Figure 2b. We note that treating PbS NCs with TBAI and CTAB results in an NC surface that is

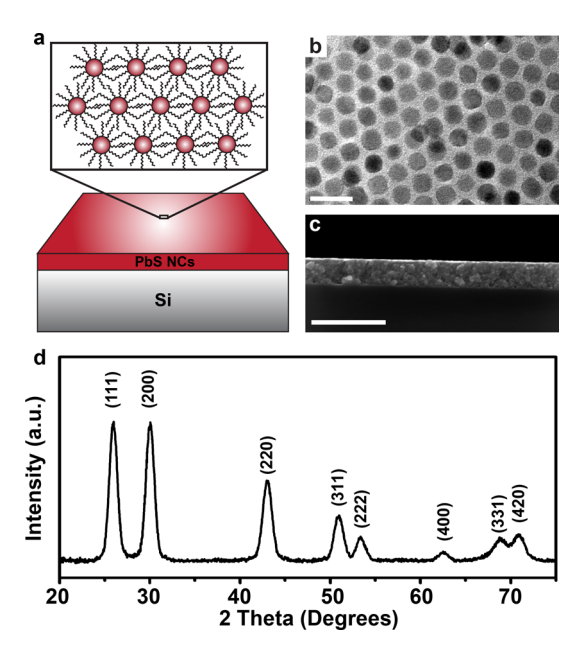


Figure 1. (a) Schematic of a PbS nanocrystal solid thin film on a silicon substrate. (b) A transmission electron microscopy image of 8.2 \pm 0.7 nm PbS nanocrystals with native oleic acid ligands (the scale bar is 20 nm). (c) Cross-sectional scanning electron microscopy image showing a nanocrystal solid thin film that consists of 8.2 nm PbS nanocrystals with I $^-$ ligands (the scale bar is 500 nm). (d) X-ray diffraction pattern of an 8.2 nm PbS nanocrystal solid thin film with oleic acid ligands.

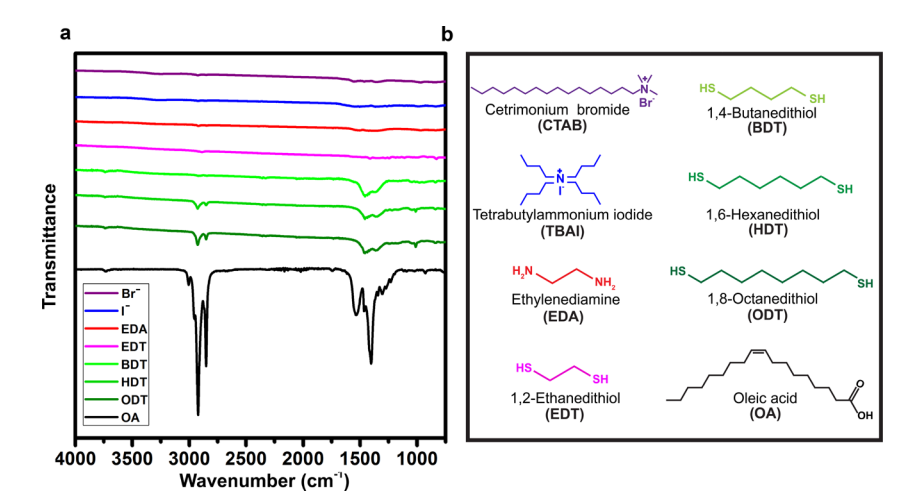


Figure 2. (a) Fourier transform infrared spectra of PbS nanocrystal solids with various ligands. (b) The chemical structure of the molecules used during ligand exchange. Note that treating PbS nanocrystals with tetrabutylammonium iodide (TBAI) and cetrimonium bromide (CTAB) results in nanocrystal surface terminations of I^- and Br^- , respectively [refs 16 and 32].

terminated with I⁻ and Br⁻, respectively (*i.e.*, the bulky organic component of these molecules washes away during the ligand exchange process).^{7,16,32} For simplicity purposes, we refer to these as I⁻ and Br⁻ ligands throughout this paper. Fourier transform infrared spectroscopy measurements confirm the success of these ligand exchanges (Figure 2a). The absence of the native OA ligands is indicated by the lack of COO⁻ and C=C absorptions, which are at 1500–1700 cm⁻¹, in all ligand exchanged samples.

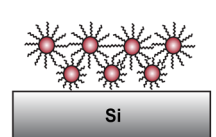
To prepare high-quality film for thermal conductivity measurements, we carried out the solid-state ligand exchange process using a layer-by-layer (LBL) approach (Figure 3a). 30,33,34 Each layer was prepared in three steps: (a) depositing a thin layer of PbS NCs with OA ligands via spin coating; (b) immersing the NC solid film in a solution containing the desired ligand (typically 30 s) and spinning dry; (c) removing unbound ligand molecules by repeatedly flooding the NC solid film with pure solvent and spinning dry. Depending on the NC diameter and ligand choice, each layer deposition resulted in a NC solid thin film of 10-25 nm. This deposition process was then repeated 6-10 times to yield thicker films (100-180 nm) that are appropriate for thermal conductivity measurements. Films prepared by this approach exhibited excellent film quality with minimal porosity/cracking (Figure 3b). In contrast, NC solid films prepared via one-time solid-state ligand exchange on thick films exhibited extensive/deep cracking that made them unsuitable for transport measurements (Figure S6).

We first investigate the effect of the ligand's binding group on the NC solid thermal conductivity (Figure 4). This is motivated by past thermal transport studies on a closely related cousin to colloidal NCs, self-assembled monolayer (SAM) junctions. SAMs are molecular monolayers adsorbed onto planar solid surfaces and prior work has shown an increasing thermal

 Spin coat a thin layer of PbS NCs with OA ligands.



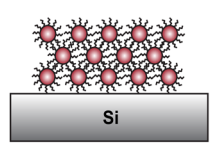
3. Spin coat a thin layer of PbS NCs with OA ligands.



2. Exchange OA with new short ligands.



4. Repeat steps 2 and 3 to yield a dense thick film.



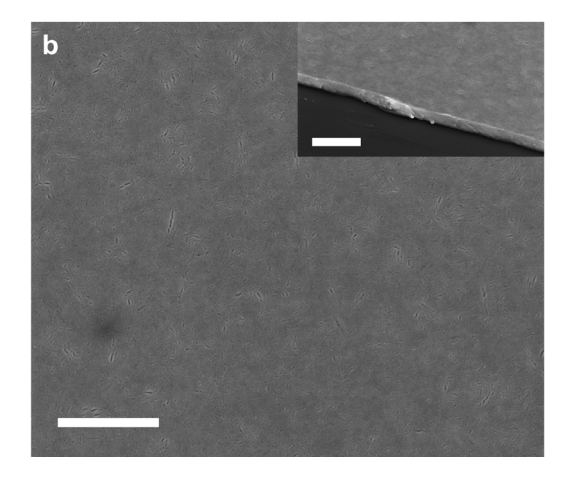


Figure 3. (a) Schematic illustrating the solid-state, layer-by-layer ligand exchange technique used to prepare nanocrystal (NC) solid films. This layer-by-layer technique minimizes film cracking during exchange of the long oleic acid (OA) ligands with new short ligands. (b) Scanning electron microscopy image of a 3.3 nm PbS NC solid with ethanedithiol ligands. The inset in part (b) shows an angled view of the NC solid film that confirms dense NC packing throughout the film thickness. The scale bar in both images is 1 μ m.

interface conductance as the binding strength between the SAM molecules and solid surface increases. 35,36

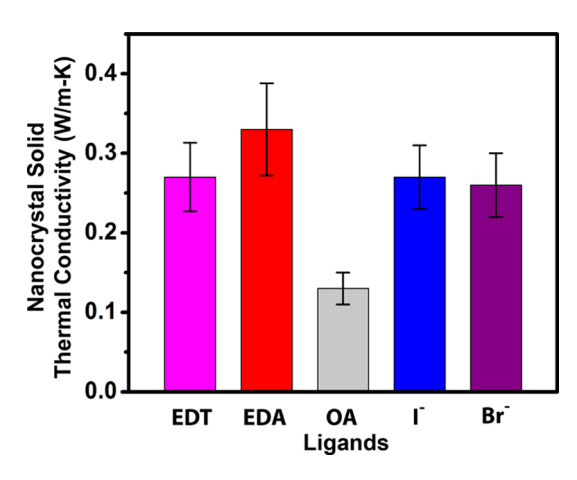
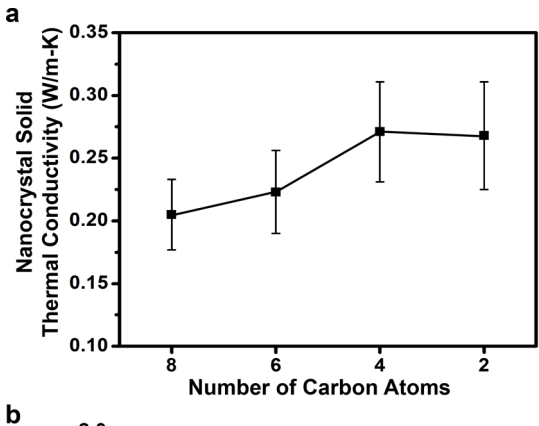
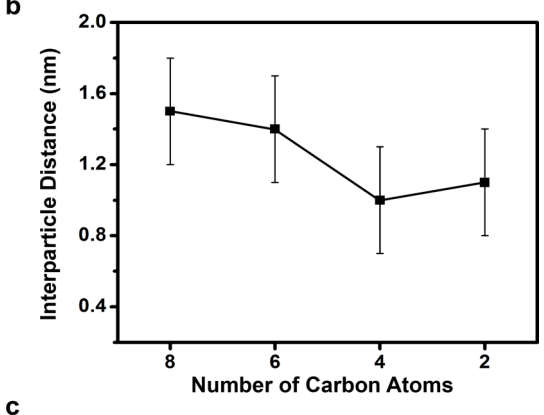


Figure 4. Thermal conductivity of 3.3 nm PbS nanocrystal solids with ethanedithiol (EDT), ethylenediamine (EDA), oleic acid (OA), I^- , and Br^- ligands.

In effect, we ask ourselves whether this correlation between binding strength and thermal transport can be realized in the more complex structure of NC solids. To investigate this, we compare the thermal conductivity of 3.3 nm diameter PbS NC solids with EDA and EDT ligands. These two ligands have identical backbones, but different binding groups: amine groups for EDA and thiol groups for EDT. Both of these groups form covalent bonds to PbS NCs, although it is known that the thiol group forms a stronger bond than the amine group.³⁸ Interestingly, we find that PbS NC solids with EDT ligands have a lower thermal conductivity than with EDA ligands (Figure 4). This contrasts with data on SAM junctions, in which the thermal conductance through strong thiol-Au bonds is notably larger than the thermal conductance through weaker amine-Au bonds. 35 To expand upon this binding group motif, we also prepared PbS NC solids with halide ligands (Br and I). These ligands form ionic bonds to the NC surface, of which the PbS-Br bond is known to be the stronger of the two.³⁰ We find that the thermal conductivity of NC solids with these two ligands are essentially equivalent and do not reflect the prediction based on bond strength as well. Based on these experimental observations, we conclude that the thermal conductance of the NC core-ligand interface (i.e., the binding strength between the NC core and ligand) does not dominate thermal transport in NC solids. As based upon our EMA modeling (see below), we hypothesize that the ligand-ligand interface between neighboring NCs is the critical interface for thermal transport in NC solids.

We next study the effect of ligand length by using a series of alkanedithiol ligands with 2, 4, 6, and 8 carbon atoms (*i.e.*, EDT, BDT, HDT, and ODT, respectively) on 3.3 nm PbS NC solids. As the ligand backbone decreased from 8 carbon atoms to 4 carbon atoms, the NC solid thermal conductivity increased from 0.20 W/m-K to 0.27 W/m-K (Figure 5a). We attribute this trend to a reduction of interparticle distance, which increases the





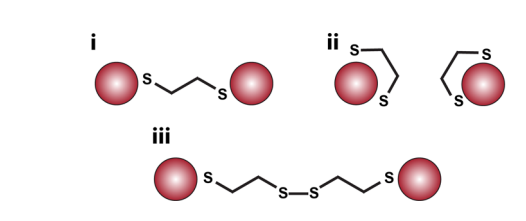
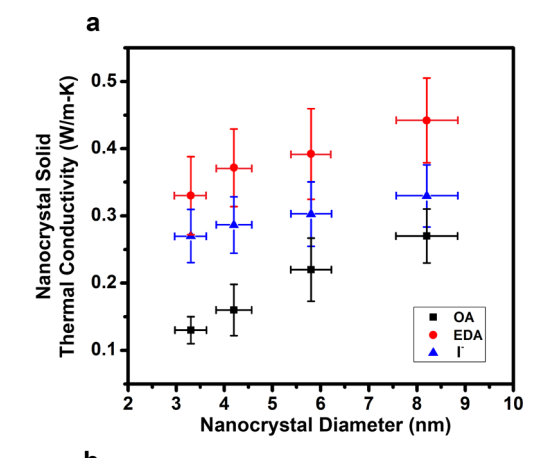


Figure 5. (a) Thermal conductivity of 3.3 nm PbS nanocrystal solids with alkanedithiol ligands of varying backbone length. (b) Interparticle distance of 3.3 nm PbS nanocrystal solids with alkanedithiol ligands of varying backbone length. (c) Schematic of various binding possibilities for ethanedithiol in nanocrystal solids: (i) bridging, (ii) bidentate, (iii) dimerized.

NC core volume fraction in the solids. It is not surprising that this increases the thermal conductivity of the NC solid because the thermal conductivity of PbS is an order of magnitude higher than hydrocarbons. 39,40 We also performed X-ray reflectivity (XRR) to determine the mass densities of the NC solids with varying ligands, and then converted these values into interparticle distances using geometric arguments (see Supporting Information). We found that our interparticle distance measurements agree to within experimental uncertainty with much more sophisticated synchrotron X-ray scattering measurements.²⁵ Our interparticle distance trend shows an inverse correlation with our measured thermal conductivities (Figures 5a and 5b), which supports our conclusion that interparticle distance is an important parameter affecting the thermal conductivity of NC solids. Interestingly, our results show no thermal conductivity increase as the ligand backbone is further reduced from 4 to 2 carbon atoms (BDT and EDT, respectively). While counterintuitive, we find that this thermal conductivity result still mirrors our findings on interparticle distance, which reveal approximately equivalent interparticle distances for BDT and EDT. We hypothesize that this change in trend for interparticle distance and thermal conductivity originates from a change in chemical binding motifs (Figure 5c). Similar property trend changes for varying alkanedithiol lengths have been observed in other works as well.^{25,33} Past studies have suggested that dithiol ligands preferentially bridge neighboring NCs (part i in Figure 5c).^{25,41,42} Since our measured interparticle distances for NC solids with ODT, HDT, and BDT are comparable to that of the corresponding molecular lengths,²⁵ we hypothesize that NC bridging occurs in these cases. However, in the case of EDT, the interparticle distance is notably longer than the molecular length. This implies an alternative chemical binding motif; both bidentate binding^{25,33,34} and dimerized binding^{43,44} (parts ii and iii, respectively, in Figure 5c) have been identified as possible binding arrangements for EDT in NC solids. We also performed XRR measurements on NC solids with EDA ligands and found very short interparticle distances (i.e., \sim 0.7 nm). This result suggests that EDA likely bridges NCs and provides an explanation as to why EDA ligands yield a higher NC solid thermal conductivity than EDT (Figure 4).

We next study the relative impact of surface chemistry on the thermal conductivity of NC solids with varying NC diameter. As a baseline, we first measure the thermal conductivity of PbS NC solids with their native OA ligands. We find that as the NC diameter increases from 3.3 to 8.2 nm, the thermal conductivity increases from 0.13 to 0.27 W/m-K, which agrees with measurements by Ong et al. 13 It is worth noting that our thermal conductivity measurements use the 3ω technique, 45-47 which is comparatively simpler to implement than Ong's frequency-domain thermal reflectance technique. This data demonstrates that nanocrystal solid thermal conductivity measurements should be accessible to a broader range of research laboratories. To study the combined effect of NC diameter and surface chemistry, we prepare each of these NC solids with I⁻ and EDA ligands and find that the thermal conductivity increases for all diameters (Figure 6a). This is consistent with the relationship between thermal conductivity and interparticle distance that we identified earlier. It is also possible that these ligand choices lead to higher effective thermal conductivities in the ligand matrix. In addition, we find that the relative thermal conductivity increase $(k/k_{\rm NC-OA})$ is greater for smaller diameter NC solids than for larger diameters ones (Figure 6b). This trend is consistent with the fact that the ligands make up a greater volume fraction of the NC solid as the NC diameter decreases, and should therefore have a more substantial effect for smaller diameters. We achieve relative thermal conductivity



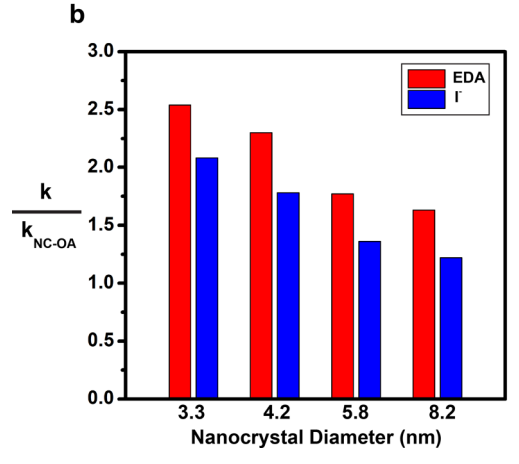
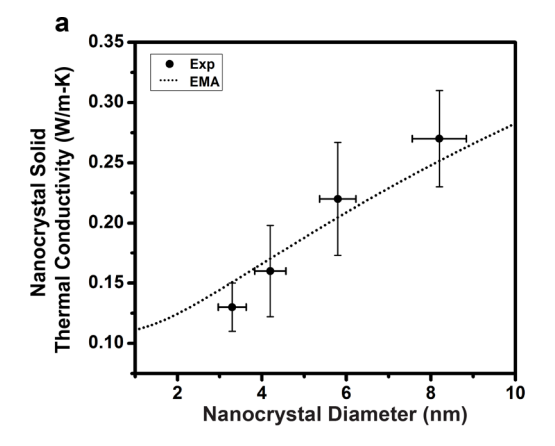


Figure 6. (a) The thermal conductivity of PbS nanocrystal solids with oleic acid (OA), ethylenediamine (EDA), and I ligands as a function of nanocrystal diameter. (b) The relative increase of thermal conductivity $(k/k_{\rm NC-OA})$ in PbS nanocrystal solids with ethylenediamine and I ligands and varying nanocrystal diameter. The data in part (b) is normalized to the thermal conductivity of PbS nanocrystal solids with OA ligands, $k_{\rm NC-OA}$.

increases of up to 150%, which improves upon the 50% increase demonstrated in prior work. 13 While data in prior work suggests that NC diameter is the parameter that most affects NC solid thermal conductivity, 13,21,22 our findings demonstrate that surface chemistry can have an even larger impact. For example, consider the case of a 3.3 nm PbS NC solid with OA ligands, which has a thermal conductivity of 0.13 W/m-K. Increasing the NC diameter to 8.2 nm and keeping the native OA ligands leads to a thermal conductivity of 0.27 W/m-K. In contrast, keeping the same 3.3 nm diameter, but exchanging the OA with EDA leads to an even higher thermal conductivity of 0.33 W/m-K. Naturally, the effect of NC diameter and surface chemistry can be combined; we achieve our lowest thermal conductivity in 3.3 nm PbS with OA ligands and our highest thermal conductivity in 8.2 nm PbS with EDA ligands. Overall, we find that within our size range (\sim 3–8 nm), the thermal conductivity of NC solids can be varied from approximately 0.1-0.4 W/m-K, which demonstrates a moderately larger range of possibilities than prior work.¹³

To gauge how this range of NC solid thermal conductivities can be further expanded, we use an EMA model to fit our data on PbS NCs with OA ligands and then perform a sensitivity analysis on the various model input parameters. Since thermal interface conductances significantly impact the thermal conductivity of nanocomposites, we incorporate this factor by using the EMA model proposed by Hasselman and Johnson.⁴⁸ This EMA model calculates the thermal conductivity of a composite by accounting for the constituent volume fractions, constituent thermal conductivities, and thermal interface conductance between the constituents. To apply the EMA model to our NC solid, we consider a nanocomposite consisting of NC cores in a ligand matrix. Figure 7a shows the EMA model fit to our PbS NC solids with OA ligands and varying diameter, which shows good agreement. In this fit we use 2 W/m-K, 0.13 W/m-K, 2.5 nm, and 220 MW/m²-K for the NC core thermal conductivity (k_{NC}) , ligand matrix thermal conductivity (k_m) , interparticle distance, and NC core-ligand thermal interface conductance (G), respectively. Our choice of these input parameters for the model is based upon results in the literature. 13,25,35,49 Additional details on our EMA model implementation can be found in the Supporting Information.

To study the relative impact of each parameter (k_{NC} , G, and k_m) on NC solid thermal conductivity, we independently vary each parameter while holding the other two constant (Figure 7b). We find that k_m has the largest impact, G has a moderate impact, and $k_{\rm NC}$ has a small impact. As k_m , G, and $k_{\rm NC}$ are each varied by a factor of 5, we calculate changes in NC solid thermal conductivity of 386%, 27%, and 4%, respectively. The insensitivity to $k_{\rm NC}$ is not surprising given that it is an order of magnitude larger than k_m and the core-ligand interfaces further restrict this thermal pathway. Prior experimental work has also found that NC solid thermal conductivity is largely independent of $k_{\rm NC}$. The fact that the NC solid thermal conductivity sensitivity is much greater to k_m than G means the thermal conductance of the ligand matrix is more important than the thermal conductance of the NC core-ligand interface. This possibly explains why we did not experimentally observe an increase in NC solid thermal conductivity as we increased the NC coreligand binding strength (which, according to literature on solid-SAM junctions, should have increased the NC core-ligand thermal interface conductance). It is also worth noting that the thermal interface conductance of an individual solid-SAM interface only changes by about a factor of 4 as the solid-SAM bond is changed from van der Waals to covalent.35,49 According to our EMA model, this would correspond to an ~20% change in NC thermal conductivity. Given that the NC core-ligand bond strength is varied in a much narrower range during our experiments, any thermal conductivity



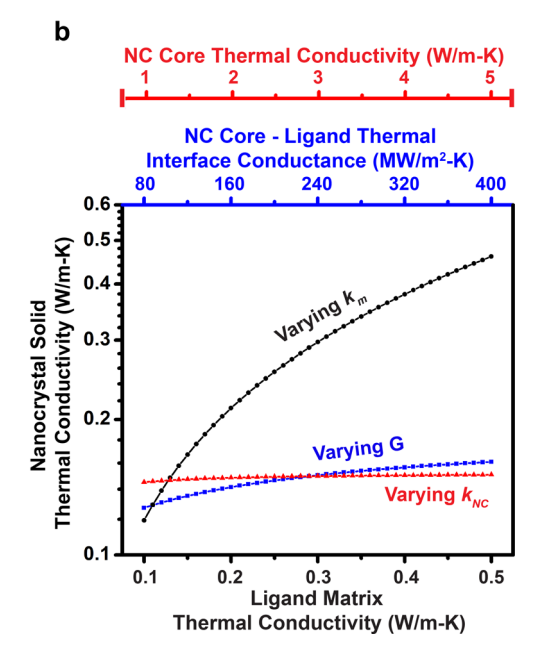


Figure 7. (a) Effective medium approximation (EMA) model results and corresponding experimental data for the thermal conductivity of PbS nanocrystal (NC) solids with oleic acid ligands and varying diameter. (b) Sensitivity analysis on the EMA model for 3.3 nm PbS NC solids with three independent parameters: NC core thermal conductivity ($k_{\rm NC}$, red triangles), NC core-ligand thermal interface conductance (G, blue squares), and ligand matrix thermal conductivity (k_{mr} , black spheres).

changes arising from NC core-ligand bond strength were likely small, which explains why our measurements did not detect significant changes.

Since k_m affects NC solid thermal conductivity the most, determining ways to increase or decrease k_m is a promising route to achieve an expanded thermal conductivity range beyond that demonstrated in the present work. It is notable that the maximum thermal conductivity for the matrix used in our EMA sensitivity analysis is only 0.5 W/m-K, which is comparable to typical thermal insulators. Consequently, there should be room to increase the thermal conductivity of the ligand matrix, and by extension, increase the thermal conductivity of the NC solid. This finding inspires us to hypothesize why thermal transport in the ligand matrix

is poor to begin with. If we consider heat flow between two neighboring NCs, there are three interfaces: a NC core-ligand interface, a ligand-ligand interface, and then another NC core-ligand interface. Whereas the NC core-ligand interfaces are generally strong covalent or ionic bonds, the ligand-ligand interface is characterized by weak van der Waals forces. Several studies on polymers, 50 molecular crystals, 51 and carbon nanotube polymer composites⁵² have identified weak van der Waals interactions as rate-limiters for heat transfer. We hypothesize that this is also true for thermal transport in NC solids. We note that there is no analogous ligand-ligand interface in solid-SAM-solid structures, which may explain why the solid-molecule binding strength plays a significant thermal transport role in SAMs, but not necessarily in NC solids.

We hypothesize that two possible ways to increase the thermal conductivity of NC solids are (i) chemically cross-linking the NC ligands to strengthen the ligandligand interaction, (ii) eliminating the ligand-ligand interaction by bridging neighboring NCs with bifunctional ligands. The first concept has been demonstrated in a recent study on amorphous polymer blends; by introducing appropriately engineered cross-linkers, the thermal conductivity of the polymer blend was increased by a factor of 7.53 The second approach has been highly sought after in studies to improve charge transport in NC solids, 42,54,55 and motivated our choice of bifunctional ligands (e.g., dithiols and diamine) in this study. However, this approach will likely prove complex because NC surfaces are highly curved, which leads to nonuniform distances between neighboring NCs. This curvature limits the surface area upon which ligand bridging

can occur and may explain why we only observed moderately higher thermal conductivities with bridging ligands (e.g., EDA) relative to nonbridging ligands (e.g., EDT and I^-). Using colloidal nanocrystals with flat surfaces (e.g., cubes) and/or more sophisticated ligand chemistries that can achieve bridging throughout the entire NC surface could prove interesting.

CONCLUSION

We have systematically explored the effect of ligand length, ligand binding group, and NC diameter on thermal transport in colloidal PbS NC solids. The primary effect of decreasing ligand length and/or increasing NC diameter is to increase the NC solid thermal conductivity by decreasing the volume fraction of the thermally insulating ligand matrix. Varying the ligand binding strength to the NC core does not lead to significant effects on thermal transport, which contrasts with literature on solid-SAM-solid junctions. We find that the choice of ligands can affect the thermal conductivity by up to a factor of 2.5 and that the thermal conductivity of NC solids can be varied by an overall factor of 4, from \sim 0.1 to 0.4 W/m-K. By combining our experimental observations with EMA modeling, we identified the ligand-ligand interface between neighboring NCs as a critical interface for heat transfer. We then suggested ways to modify this interface and possibly increase NC solid thermal conductivity. Identifying ways to increase thermal conductivity will be beneficial to NC solid applications in electronics and optoelectronics, for which heat dissipation is important to device performance and lifetime. On the other hand, the naturally low thermal conductivities of NC solids bode well for NC solid-based thermoelectrics.

MATERIALS AND METHODS

Materials and Equipment. Lead oxide (99.999%), bis-(trimethylsilyl)sulfide (TMS, synthesis grade), oleic acid (OA, 90%), 1-octadecene (ODE, 90%), tetrabutylammonium iodide (TBAI, 98%+), cetrimonium bromide (CTAB, 99%), 1,2-ethanedithiol (EDT, 98%+), 1,4-butanedithiol (BDT, 97%+), 1,6hexanedithiol (HDT, 96%+), 1,8-octanedithiol (ODT, 97%+), ethylenediamine (EDA, 99%), methanol (anhydrous 99.8%), acetonitrile (anhydrous 99.8%), octane (98%), were purchased from Sigma-Aldrich and used as received. Sample imaging was done with transmission electron microscopy (TEM, Tecnai F20) and scanning electron microscopy (SEM, Nova 200 NanoLab FEI). The X-ray diffraction was taken on high resolution PANalytical X-ray diffractometer, with Cu $K\alpha$ X-ray source operating at 40 kV and 40 mA. The X-ray reflectivity measurements were also done using the PANalytical X-ray diffractometer. Fourier transform infrared spectroscopy measurements were done using a Thermo Nicolet 6700 system equipped with Smart SAGA accessory. Thickness measurements were carried out using atomic force microscopy (Digital Instrument Dimension 3000) and profilometry (Dektek II surface profilometer). For thermal conductivity measurements, a Keithley 6221 was used as the current source and a Stanford Research Systems SR830 lock-in amplifier was used to measure the first and third harmonic voltage signals.

Nanocrystal Synthesis. PbS colloidal NCs were synthesized by employing the hot injection technique reported by Hines $et\,al.$ ³¹

with minor modifications. In a typical synthesis of 3 nm PbS NCs, 0.45 g of lead oxide was dissolved in a solvent mixture of 2 mL OA and 18 mL ODE, and degassed by heating under a vacuum at 100 °C for 2 h. After all of the solid dissolved and the solution turned transparent, the temperature was increased to 145 °C, at which point a mixture of 10 mL ODE and 210 μ L TMS was injected. The heating mantle was removed from the reaction flask right after the TMS injection, and then replaced when the temperature dropped to 100 °C. The reaction mixture was slowly cooled to \sim 30 $^{\circ}$ C with the heating mantle in place and turned off. PbS NCs were then separated from the reaction mixture by precipitating with ethanol and resuspending with hexane. This precipitation/suspension process was carried out 3 times in total. To vary NC diameter, the ratio of OA:ODE was varied; higher OA concentration led to larger diameters. The diameters of the PbS NCs used in this study were 3.3 \pm 0.3 nm, 4.2 \pm 0.4 nm, 5.8 \pm 0.4 nm and 8.2 \pm 0.7 nm (Figure S5).

Layer-by-Layer (LBL) Ligand Exchange. Ligand exchange in all NC solid films were done using a solid-state ligand exchange process in a LBL fashion. Prior to film deposition, all NCs were precipitated and resuspended an additional 3 times. The NCs were suspended in octane with a concentration of 10-15 mg/mL for the film deposition. For each layer deposition, $\sim 70~\mu$ L PbS NC suspension was dispensed onto a $20~\text{mm} \times 20~\text{mm}$ silicon substrate and spin coated at a speed of 3000~rpm for 1 min. Then, $\sim 200~\mu$ L of the ligand solution was dispensed onto the

NC solid thin film, allowed to rest for 30 s, and then removed by spin drying. The NC solid film was then flooded by $\sim\!200~\mu\text{L}$ of pure solvent and then spun dry to remove unbound ligands. The NC solid was then flooded with solvent and spun dry an additional 2 times. Depending on NC size and ligand, each layer deposition resulted in a thin film between 10–25 nm. Typically, 6–10 layers of NC solid were deposited to yield an appropriate film thickness for thermal conductivity measurements ($\sim\!100-180$ nm). Thinner films made via 2–3 layer deposition cycles ($\sim\!20-30$ nm) were used for measuring mass density via X-ray reflectivity. The ligand solutions were prepared as suggested by previous studies; 30,33 CTAB and TBAI, 30 mM in methanol; EDT, 1.7 mM in acetonitrile; BDT, 2.5 mM in acetonitrile; HDT, 4 mM in acetonitrile; and ODT, 8 mM in acetonitrile.

Film Thickness Measurement. Thickness measurements on all ligand exchanged NC solid samples were determined by profilometry measurements. NC films were scratched using tweezers and the film thickness measured at the scratch location. The film thickness was determined by averaging measured thicknesses from 3 scans at different locations. The typical thickness variation at these scratch locations was found to be less than 10 nm. NC solids with OA ligands were too soft to have their thickness measured with profilometry and were instead measured with atomic force microscopy.

Thermal Conductivity Measurement. Thermal conductivity measurements were performed using the differential 3ω method, which is a widely used technique for thin film geometries. 46,47 To prepare samples for measurement, NC solid films were first coated with a \sim 150 nm Al_2O_3 dielectric layer. Al metal lines, which function as combined heaters and thermometers, were then deposited on the samples using a shadow mask. The line dimensions in all samples were 45 μ m wide, 2.6 mm long, and 150 nm thick. An AC current was run through the Al line to operate it as a heat source and the third harmonic of the voltage response was measured to operate the Al line as a thermometer. In accordance with the differential technique, a reference sample with only dielectric layer and silicon substrate was identically prepared. The thermal response of the NC solid thin film was obtained by subtracting the thermal response of the reference sample from the experimental sample. To convert 3ω electrical signals into thermal responses, the temperature coefficient of resistance (TCR) of 3ω lines were measured using a home-built thermal stage. In this measurement, the resistances of the 3ω lines were measured at 5 different temperature points between 15 and 30 $^{\circ}$ C, and a linear fit was used to determine the slope. A detailed description of our 3ω technique implementation along with benchmark measurements on control samples can be found in the Supporting Information.

Conflict of Interest: The authors declare no competing financial interest.

Acknowledgment. This work was supported by the Young Investigator Research Program of the Air Force Office of Scientific Research through award number FA9550-13-1-0163 and by the National Science Foundation through award number CBET-1227979. We thank Emmanuel Soignard for performing the X-ray reflectivity measurements. We gratefully acknowledge the use of facilities within the LeRoy Eyring Center for Solid State Science and the Center for Solid State Electronics Research, both of which are located at Arizona State University.

Supporting Information Available: The Supporting Information is available free of charge on the ACS Publications website at DOI: 10.1021/acsnano.5b05085.

Additional microscopy images along with detailed descriptions of our interparticle distance measurements, effective medium approximation modeling, and 3ω technique implementation. (PDF)

REFERENCES AND NOTES

 Llordes, A.; Garcia, G.; Gazquez, J.; Milliron, D. J. Tunable near-Infrared and Visible-Light Transmittance in Nanocrystal-in-Glass Composites. *Nature* 2013, 500, 323–326.

- Wang, R. Y.; Feser, J. P.; Lee, J.-S.; Talapin, D. V.; Segalman, R.; Majumdar, A. Enhanced Thermopower in Pbse Nanocrystal Quantum Dot Superlattices. *Nano Lett.* 2008, 8, 2283–2288.
- Liu, M.; Ma, Y.; Wu, H.; Wang, R. Y. Metal Matrix-Metal Nanoparticle Composites with Tunable Melting Temperature and High Thermal Conductivity for Phase-Change Thermal Storage. ACS Nano 2015, 9, 1341–1351.
- Dai, X.; Zhang, Z.; Jin, Y.; Niu, Y.; Cao, H.; Liang, X.; Chen, L.; Wang, J.; Peng, X. Solution-Processed, High-Performance Light-Emitting Diodes Based on Quantum Dots. *Nature* 2014, 515, 96–99.
- Cho, K. S.; Lee, E. K.; Joo, W. J.; Jang, E.; Kim, T. H.; Lee, S. J.; Kwon, S. J.; Han, J. Y.; Kim, B. K.; Choi, B. L.; et al. High-Performance Crosslinked Colloidal Quantum-Dot Light-Emitting Diodes. Nat. Photonics 2009, 3, 341–345.
- Mcdonald, S. A.; Konstantatos, G.; Zhang, S.; Cyr, P. W.; Klem, E. J.; Levina, L.; Sargent, E. H. Solution-Processed PbS Quantum Dot Infrared Photodetectors and Photovoltaics. Nat. Mater. 2005, 4, 138–142.
- Chuang, C.-H. M.; Brown, P. R.; Bulović, V.; Bawendi, M. G. Improved Performance and Stability in Quantum Dot Solar Cells through Band Alignment Engineering. *Nat. Mater.* 2014, 13, 796–801.
- Oh, S. J.; Wang, Z.; Berry, N. E.; Choi, J.-H.; Zhao, T.; Gaulding, E. A.; Paik, T.; Lai, Y.; Murray, C. B.; Kagan, C. R. Engineering Charge Injection and Charge Transport for High Performance PbSe Nanocrystal Thin Film Devices and Circuits. Nano Lett. 2014, 14, 6210–6216.
- Turk, M. E.; Choi, J.-H.; Oh, S. J.; Fafarman, A. T.; Diroll, B. T.; Murray, C. B.; Kagan, C. R.; Kikkawa, J. M. Gate-Induced Carrier Delocalization in Quantum Dot Field Effect Transistors. *Nano Lett.* 2014, 14, 5948–5952.
- Liu, M.; Wang, R. Y. Phase Change Nanocomposites with Tunable Melting Temperature and Thermal Energy Storage Density. Nanoscale 2013, 5, 7234–7237.
- Fan, F.-J.; Yu, B.; Wang, Y.-X.; Zhu, Y.-L.; Liu, X.-J.; Yu, S.-H.; Ren, Z. Colloidal Synthesis of Cu₂CdSnSe₄ Nanocrystals and Hot-Pressing to Enhance the Thermoelectric Figureof-Merit. J. Am. Chem. Soc. 2011, 133, 15910–15913.
- Fan, F.-J.; Wang, Y.-X.; Liu, X.-J.; Wu, L.; Yu, S.-H. Large-Scale Colloidal Synthesis of Non-Stoichiometric Cu₂ZnSnSe4 Nanocrystals for Thermoelectric Applications. *Adv. Mater.* 2012, 24, 6158–6163.
- Ong, W.-L.; Rupich, S. M.; Talapin, D. V.; McGaughey, A. J. H.; Malen, J. A. Surface Chemistry Mediates Thermal Transport in Three-Dimensional Nanocrystal Arrays. *Nat. Mater.* 2013. 12, 410–415.
- Smith, A. R.; Yoon, W.; Heuer, W. B.; Baril, S. I. M.; Boercker, J. E.; Tischler, J. G.; Foos, E. E. Effect of Ligand Structure on the Optical and Electronic Properties of Nanocrystalline PbSe Films. J. Phys. Chem. C 2012, 116, 6031–6037.
- Lee, J.-S.; Kovalenko, M. V.; Huang, J.; Chung, D. S.; Talapin, D. V. Band-Like Transport, High Electron Mobility and High Photoconductivity in All-Inorganic Nanocrystal Arrays. Nat. Nanotechnol. 2011, 6, 348–352.
- Tang, J.; Kemp, K. W.; Hoogland, S.; Jeong, K. S.; Liu, H.; Levina, L.; Furukawa, M.; Wang, X.; Debnath, R.; Cha, D. Colloidal-Quantum-Dot Photovoltaics Using Atomic-Ligand Passivation. *Nat. Mater.* 2011, 10, 765–771.
- Sun, Y.; Fang, H.; Pan, L.; Han, M.; Xu, S.; Wang, X.; Xu, B.; Wu, Y. Impact of Surface-Bound Small Molecules on the Thermoelectric Property of Self-Assembled Ag₂Te Nanocrystal Thin Films. Nano Lett. 2015, 15, 3748–3756.
- Kovalenko, M. V.; Scheele, M.; Talapin, D. V. Colloidal Nanocrystals with Molecular Metal Chalcogenide Surface Ligands. Science 2009, 324, 1417–1420.
- Giansante, C.; Infante, I.; Fabiano, E.; Grisorio, R.; Suranna, G. P.; Gigli, G. Darker-Than-Black" PbS Quantum Dots: Enhancing Optical Absorption of Colloidal Semiconductor Nanocrystals via Short Conjugated Ligands. J. Am. Chem. Soc. 2015, 137, 1875–1886.
- Gao, Y.; Aerts, M.; Sandeep, C. S. S.; Talgorn, E.; Savenije, T. J.; Kinge, S.; Siebbeles, L. D. A.; Houtepen, A. J. Photoconductivity of PbSe Quantum-Dot Solids: Dependence

ACSNANO www.acsnano.org

- on Ligand Anchor Group and Length. ACS Nano 2012, 6, 9606–9614.
- Zanjani, M. B.; Lukes, J. R. Phonon Dispersion and Thermal Conductivity of Nanocrystal Superlattices Using Three-Dimensional Atomistic Models. J. Appl. Phys. 2014, 115, 143515.
- Ong, W.-L.; Majumdar, S.; Malen, J. A.; McGaughey, A. J. H. Coupling of Organic and Inorganic Vibrational States and Their Thermal Transport in Nanocrystal Arrays. J. Phys. Chem. C 2014, 118, 7288–7295.
- Szendrei, K.; Cordella, F.; Kovalenko, M. V.; Böberl, M.; Hesser, G.; Yarema, M.; Jarzab, D.; Mikhnenko, O. V.; Gocalinska, A.; Saba, M.; et al. Solution-Processable near-Ir Photodetectors Based on Electron Transfer from PbS Nanocrystals to Fullerene Derivatives. Adv. Mater. 2009, 21, 683–687.
- Gao, J.; Perkins, C. L.; Luther, J. M.; Hanna, M. C.; Chen, H.-Y.; Semonin, O. E.; Nozik, A. J.; Ellingson, R. J.; Beard, M. C. N-Type Transition Metal Oxide as a Hole Extraction Layer in PbS Quantum Dot Solar Cells. *Nano Lett.* 2011, 11, 3263–3266.
- Weidman, M. C.; Yager, K. G.; Tisdale, W. A. Interparticle Spacing and Structural Ordering in Superlattice PbS Nanocrystal Solids Undergoing Ligand Exchange. *Chem. Mater.* 2015, 27, 474–482.
- Zherebetskyy, D.; Scheele, M.; Zhang, Y.; Bronstein, N.; Thompson, C.; Britt, D.; Salmeron, M.; Alivisatos, P.; Wang, L.-W. Hydroxylation of the Surface of PbS Nanocrystals Passivated with Oleic Acid. Science 2014, 344, 1380–1384.
- Podsiadlo, P.; Krylova, G.; Lee, B.; Critchley, K.; Gosztola, D. J.; Talapin, D. V.; Ashby, P. D.; Shevchenko, E. V. The Role of Order, Nanocrystal Size, and Capping Ligands in the Collective Mechanical Response of Three-Dimensional Nanocrystal Solids. J. Am. Chem. Soc. 2010, 132, 8953– 8960
- Cademartiri, L.; Montanari, E.; Calestani, G.; Migliori, A.; Guagliardi, A.; Ozin, G. A. Size-Dependent Extinction Coefficients of PbS Quantum Dots. J. Am. Chem. Soc. 2006, 128, 10337–10346.
- Konstantatos, G.; Howard, I.; Fischer, A.; Hoogland, S.; Clifford, J.; Klem, E.; Levina, L.; Sargent, E. H. Ultrasensitive Solution-Cast Quantum Dot Photodetectors. *Nature* 2006, 442, 180–183.
- Brown, P. R.; Kim, D.; Lunt, R. R.; Zhao, N.; Bawendi, M. G.; Grossman, J. C.; Bulović, V. Energy Level Modification in Lead Sulfide Quantum Dot Thin Films through Ligand Exchange. ACS Nano 2014, 8, 5863–5872.
- Hines, M. A.; Scholes, G. D. Colloidal PbS Nanocrystals with Size-Tunable near-Infrared Emission: Observation of Post-Synthesis Self-Narrowing of the Particle Size Distribution. Adv. Mater. 2003, 15, 1844–1849.
- Ning, Z.; Voznyy, O.; Pan, J.; Hoogland, S.; Adinolfi, V.; Xu, J.; Li, M.; Kirmani, A. R.; Sun, J.-P.; Minor, J.; et al. Air-Stable N-Type Colloidal Quantum Dot Solids. Nat. Mater. 2014, 13, 822–828.
- Lynch, J.; Kotiuga, M.; Doan-Nguyen, V. V. T.; Queen, W. L.; Forster, J. D.; Schlitz, R. A.; Murray, C. B.; Neaton, J. B.; Chabinyc, M. L.; Urban, J. J. Ligand Coupling Symmetry Correlates with Thermopower Enhancement in Small-Molecule/Nanocrystal Hybrid Materials. ACS Nano 2014, 8. 10528–10536.
- Luther, J. M.; Law, M.; Song, Q.; Perkins, C. L.; Beard, M. C.; Nozik, A. J. Structural, Optical, and Electrical Properties of Self-Assembled Films of Pbse Nanocrystals Treated with 1,2-Ethanedithiol. ACS Nano 2008, 2, 271–280.
- Losego, M. D.; Grady, M. E.; Sottos, N. R.; Cahill, D. G.; Braun, P. V. Effects of Chemical Bonding on Heat Transport across Interfaces. *Nat. Mater.* 2012, 11, 502–506.
- O'Brien, P. J.; Shenogin, S.; Liu, J.; Chow, P. K.; Laurencin, D.; Mutin, P. H.; Yamaguchi, M.; Keblinski, P.; Ramanath, G. Bonding-Induced Thermal Conductance Enhancement at Inorganic Heterointerfaces Using nanomolecular Monolayers. *Nat. Mater.* 2013, *12*, 118–122.
- 37. Love, J. C.; Estroff, L. A.; Kriebel, J. K.; Nuzzo, R. G.; Whitesides, G. M. Self-Assembled Monolayers of Thiolates

- on Metals as a Form of Nanotechnology. *Chem. Rev.* **2005**, *105*. 1103–1170.
- Lee, S.-M.; Jun, Y.-W.; Cho, S.-N.; Cheon, J. Single-Crystalline Star-Shaped Nanocrystals and Their Evolution: Programming the Geometry of Nano-Building Blocks. J. Am. Chem. Soc. 2002, 124, 11244–11245.
- Thermal Conductivity Graphs for C8 to C28 Compounds. In Handbook of Thermal Conductivity; Carl, L. Y., Ed.; Gulf Professional Publishing: Houston, TX, 1995; Vol. 3, pp 1–363.
- Skelton, J. M.; Parker, S. C.; Togo, A.; Tanaka, I.; Walsh, A. Thermal Physics of the Lead Chalcogenides PbS, PbSe, and PbTe from First Principles. *Phys. Rev. B: Condens. Matter Mater. Phys.* 2014, 89, 205203.
- Talapin, D. V.; Lee, J.-S.; Kovalenko, M. V.; Shevchenko, E. V. Prospects of Colloidal Nanocrystals for Electronic and Optoelectronic Applications. Chem. Rev. 2010, 110, 389– 458
- Koleilat, G. I.; Levina, L.; Shukla, H.; Myrskog, S. H.; Hinds, S.; Pattantyus-Abraham, A. G.; Sargent, E. H. Efficient, Stable Infrared Photovoltaics Based on Solution-Cast Colloidal Quantum Dots. ACS Nano 2008, 2, 833–840.
- Joo, S. W.; Han, S. W.; Kim, K. Multilayer Formation of 1,2-Ethanedithiol on Gold: Surface-Enhanced Raman Scattering and Ellipsometry Study. *Langmuir* 2000, 16, 5391– 5396.
- 44. Qu, D.; Kim, B.-C.; Lee, C.-W. J.; Uosaki, K. 1, N-Alkanedithiol (N= 2, 4, 6, 8, 10) Self-Assembled Monolayers on Au (111): Electrochemical and Theoretical Approach. *Bull. Korean Chem. Soc.* **2009**, *30*, 2549–2554.
- 45. Cahill, D. G. Thermal Conductivity Measurement from 30 to 750 K: The 3ω Method. *Rev. Sci. Instrum.* **1990**, *61*, 802-808.
- 46. Lee, S.-M.; Cahill, D. G. Heat Transport in Thin Dielectric Films. J. Appl. Phys. 1997, 81, 2590–2595.
- Borca-Tasciuc, T.; Kumar, A. R.; Chen, G. Data Reduction in 3ω Method for Thin-Film Thermal Conductivity Determination. Rev. Sci. Instrum. 2001, 72, 2139–2147.
- Hasselman, D.; Johnson, L. F. Effective Thermal Conductivity of Composites with Interfacial Thermal Barrier Resistance. J. Compos. Mater. 1987, 21, 508–515.
- Wang, Z.; Carter, J. A.; Lagutchev, A.; Koh, Y. K.; Seong, N.-H.; Cahill, D. G.; Dlott, D. D. Ultrafast Flash Thermal Conductance of Molecular Chains. Science 2007, 317, 787–790.
- Shen, S.; Henry, A.; Tong, J.; Zheng, R.; Chen, G. Polyethylene Nanofibres with Very High Thermal Conductivities. Nat. Nanotechnol. 2010, 5, 251–255.
- Andersson, O.; Soldatov, A.; Sundqvist, B. Thermal Conductivity of C60 at Pressures up to 1 GPa and Temperatures in the 50 to 300 K Range. *Phys. Rev. B: Condens. Matter Mater. Phys.* 1996, 54, 3093–3100.
- Marconnett, A. M.; Yamamoto, N.; Panzer, M. A.; Wardle,
 B. L.; Goodson, K. E. Thermal Conduction in Aligned Carbon Nanotube-Polymer Nanocomposites with High Packing Density. ACS Nano 2011, 5, 4818–4825.
- Kim, G.-H.; Lee, D.; Shanker, A.; Shao, L.; Kwon, M. S.; Gidley, D.; Kim, J.; Pipe, K. P. High Thermal Conductivity in Amorphous Polymer Blends by Engineered Interchain Interactions. Nat. Mater. 2015, 14, 295–300.
- 54. Yu, D.; Wang, C.; Guyot-Sionnest, P. N-Type Conducting Cdse Nanocrystal Solids. *Science* **2003**, *300*, 1277–1280.
- Müller, K. H.; Wei, G.; Raguse, B.; Myers, J. Three-Dimensional Percolation Effect on Electrical Conductivity in Films of Metal Nanoparticles Linked by Organic Molecules. *Phys. Rev. B:* Condens. Matter Mater. Phys. 2003, 68, 155407.